The effect of pore geometry in constitutive hysteretic models for unsaturated water flow

Mariangeles Soldi, Luis Guarracino, Damien Jougnot

The effect of pore geometry in constitutive hysteretic models for unsaturated water flow

M. Soldi[1*], L. Guarracino[1] and D. Jougnot[2]

[1]Facultad de Ciencias Astronómicas y Geofísicas, Universidad Nacional de La Plata, Consejo Nacional de Investigaciones Científicas y Técnicas, La Plata, Argentina

[2]Sorbonne Université, CNRS, EPHE, UMR 7619 METIS, 75005, Paris, France

[*]E-mail: msoldi@fcaglp.unlp.edu.ar

This paper has been published in Environmental Fluid Mechanics:
Soldi, M., Guarracino, L. and Jougnot, D. (2022) The effect of pore geometry in constitutive hysteretic models for unsaturated water flow. Environmental Fluid Mechanics.
https://doi.org/10.1007/s10652-022-09891-0

Abstract

Water flow in porous media is strongly controlled by the microscale structure of the pore space. Therefore, understanding the dynamics at pore scale is fundamental to better estimate and describe the hydraulic properties and phenomena associated to water flow which are observed in a macroscale such as field or laboratory experiments. Pore geometry plays a key role since its variations cause modifications in hydraulic behaviour at the macroscale. In this study, we develop a new analytical model which represents the pore space of a medium as a bundle of tortuous sinusoidal capillary tubes with periodic pore throats and a fractal pore-size distribution. This model is compared with a previous model of straight constrictive capillary tubes in order to analyze the effect of pore geometry on hydraulic properties under partially saturated conditions. The comparison of the constitutive models shows that macroscopic hydraulic properties, porosity and permeability, present the strongest differences due to changes in the pore geometry. Nonetheless, no variations are observed in the relative hydraulic properties, effective saturation and relative permeability. The new model has been tested with experimental data consisting on sets of porosity-permeability, water content-pressure head, conductivity-pressure head, and hysteretic water content-pressure values. In all cases, the model is able to satisfactorily reproduce the data. This new analytical model presents an improvement over the previous model since the smoother variation of the pore radii allows a more realistic representation of the porous medium.

Article Highlights

- New constitutive model to describe hydraulic properties of porous media.
- Variations in pore geometry significantly influence porosity and permeability estimates.
- The physically-based model has analytical closed-form expressions whose predictions are consistent with laboratory data.

Keywords: Hydraulic Properties, Pore geometry, Hysteresis, Vadose Zone

1 Introduction

Flow and transport properties observed and measured in field or laboratory experiments are significantly influenced by the structure of porous media at the microscale. The pore space structure in which water flow occurs can be extremely irregular and complex for a real porous medium and plays a key role in the description of those hydraulic properties. In fact, the irregularities within the pore structure (i.e. constrictivities of the pore space) produce the hysteresis phenomenon in the hydraulic properties under unsaturated conditions of the medium (e.g. Bear, 1998; Vogel and Roth, 2001). Nonetheless, other effects can also contribute to explain the presence of this phenomenon in porous media such as contact angle effects, entrapped air and pore network connectivity (e.g. Jury et al., 1991; Pham et al., 2005). Therefore, understanding of the pore geometry and the hydraulic properties at this scale is a key feature to describe and study the hydraulic properties at the macroscale.

Several analytical and numerical models have been proposed in the literature to study water flow at pore scale, the most widely used are the capillary tube models (e.g. Burdine, 1953; Mualem, 1976a), statistical distribution of pores (Or and Tuller, 1999; Xu and Torres-Verdín, 2013) and pore-network models (e.g. Bryant and Blunt, 1992; Blunt et al., 2002; Joekar-Niasar et al., 2010; Jougnot et al., 2019). In pore-network models, the pore space is represented by a grid of pores (i.e. larger void spaces) and throats (i.e. narrow openings that connect the pores) with parametrized geometries and topology which allow to numerically simulate the flow. The irregularity of the pore geometry is represented by different cross-sectional shapes as, for example, a star, a square or a triangle (e.g. Man and Jing, 1999; Blunt et al., 2002; Joekar-Niasar et al., 2010). Based on a gamma statistical distribution of pores, Tuller et al. (1999) and Or and Tuller (1999) developed a physically based model to calculate the hydraulic conductivity as a function of matric potential. At the pore scale, they assumed an angular pore space model composed of slit-shaped spaces connected to a wider unit cell. This cell represents angular pores with different cross-sectional shapes such as a triangle, a square or a circle. Nevertheless, on the basis of capillary tube models, a wide range of models have been developed since their simplicity to describe pore properties and to derive macroscale properties. In fact, the most widely used empirical and analytical models for predicting saturation and permeability curves assuming different pore size distributions have been derived assuming a capillary tube model (Brooks and Corey, 1964; Mualem, 1976b; Van Genuchten, 1980). In a recent study, Cai et al. (2022) reviewed the fundamentals and concepts of different imbibition models developed in the framework of capillary tube models over the past 100 years. Moreover, natural porous media show statistical behaviour similar to fractal scaling laws over multiple scales, thus fractal theory has been proven as an effective tool to describe the capillary size distribution of porous media. As a result, capillary models and fractal scaling laws can provide a valuable insight on the flow of porous media and, based on them, many researchers have derived expressions of the medium properties.

Petersen (1958) proposed a model to estimate the effective diffusivity under steady state conditions and studied the quantitative effect of periodic pore constrictions on that property. To this aim, the author assumed the pore space represented by a bundle of capillaries where each pore is modelled by a hyperbola of revolution giving a pore constriction at the vertex of the hyperbola. Guarracino et al. (2014) developed a physically-based model that describes saturated and relative permeability, porosity and retention curve of a porous medium by representing the pore space as cylindrical tortuous capillary tubes with periodic fluctuations in the radius of the pores and a fractal pore size distribution. The fluctuations considered by Guarracino et al. (2014) allowed them to include the hysteresis phenomenon in the hydraulic properties. This model has recently been used by Rembert et al. (2020) to develop an analytical model to describe electrical conductivity in porous media. Wang et al. (2015) proposed an analytical model that estimates the permeability and average flow velocity in a porous medium as function of geometrical shape factors of capillaries, fractal dimensions and micro-structural parameters. In this model, the pore space is represented by a bundle of tubes with different geometrical shapes of their cross-sectional area. Soldi et al. (2017) developed a physically based analytical model to describe the hydraulic properties of a porous medium including the hysteresis phenomenon. To that end, the authors assumed a pore size distribution by following a fractal law and irregularities in the pore geometry. They introduced these irregularities in the model by considering each capillary as a cylindrical tube with periodic reductions of the capillary radius (i.e. consecutive segments of different constant radii). Recently, Stanić et al. (2020b) developed a physically based model of the water retention and hydraulic conductivity of unsaturated soils which includes capillary and adsorption effects. The authors considered capillary-based water retention and hydraulic conductivity functions based on a multifractal grain size distribution, the Young-Laplace law and Mualem's model. Later and based on fractal geometry, Xu et al. (2020) derived a pore-scale model for fluid flow through porous media and studied the hydraulic tortuosity of the media.

In the framework of capillary tube models, we derive a new analytical constitutive model that considers a more realistic pore geometry for estimating hydraulic properties under partially saturated conditions. The pore space is represented by a bundle of cylindrical capillaries whose radii follow a sinusoidal function with varying aperture along the pore length. In previous studies, the effect of changes in the geometry of the capillaries cross-sectional area has been examined for flow and medium properties (e.g. Or and Tuller, 1999; Wang et al., 2015). It is important to highlight that these studies analyzed different shapes of the capillaries but the aperture along each capillary tube is constant. In this study, we analyze the effects of pore geometry in hydraulic properties due to changes along the length of the capillaries (i.e. varying aperture). To this end, we compare the new model with the one proposed by Soldi et al. (2017) which assumes a bundle of cylindrical capillary tubes with straight periodic reductions in the pore radius. The geometry of the new model gives an advantage over that proposed by Soldi et al. (2017) due to the smooth variations of the pores radii which is a more realistic representation of a natural porous medium. Experimental descriptions of the pore geometry and fluid dynamics can be obtained due to the current developments in imaging technology which allow the direct microscopic measures by using X-ray tomography (e.g. Lindquist et al., 2000; Dong and Blunt, 2009) and high-speed cameras (e.g. Moebius and Or, 2012). It is important to remark that the main difference between the geometries of the two studied models is in the longitudinal section and that the cross-section for both is circular. For the new model, we obtain analytical closed form expressions for the saturated and relative hydraulic properties which depend on the geometrical parameters that define the pore structure, the tortuosity, the pore-size distribution and the radii of the pores. These expressions are then compared to the expressions of Soldi et al. (2017) model in order to analyze the effect of the different pore geometries in the hydraulic properties. To that aim, we perform a sensitivity analysis of these properties to changes in the geometrical parameters, and we test the estimates of the model against different sets of experimental data.

2 Constitutive models

In this section, we derive new closed-form analytical expressions for porosity, permeability, effective saturation and relative permeability in the framework of capillary tube models. First, we present the pore geometry of the model and develop some hydraulic properties which are valid for a single pore. Then, by upscaling the pore properties to a cylindrical representative elementary volume (REV) of a porous medium with a fractal pore size distribution, we obtain expressions for the hydraulic properties at the macroscale. This new model is compared with the model developed by Soldi et al. (2017). We also present in this section the pore geometry and the hydraulic properties obtained at the pore and the macroscopic scale from Soldi et al. (2017).

2.1 Pore geometry description

The constitutive model proposed by Soldi et al. (2017), from now on referred to as straight piecewise model, considers that, at the microscale, the pore structure of the medium is represented by capillary tubes with varying aperture. Each pore is conceptualized as a circular tube of radius R (m) and length l (m) with periodically straight pore throats of radius aR and length $c\lambda$ (as shown in Fig.1). The factor a is defined as the radial factor which represents the ratio in which the radius of the pore is reduced. Assuming that the pore geometry has a wavelength λ, the factor c represents the fraction of λ with the pore throat. Then, the pore radius can be expressed for one wavelength as (Soldi et al., 2017):

$$r(x) = \begin{cases} R & \text{if} \quad x \in [0, \lambda(1-c)), \\ aR & \text{if} \quad x \in [\lambda(1-c), \lambda), \end{cases} \tag{1}$$

where the factors a and c vary between 0 and 1. Note that the model also considers that this geometry is replicated along a capillary tube and that the length of the tube contains an integer number M of wavelengths.

Under similar hypotheses and the previously defined a and c factors, a new pore geometry is considered for each capillary tube. While the cross-section of the pore is circular as in the previous geometry, the radius of each tube is variable in the constrictive

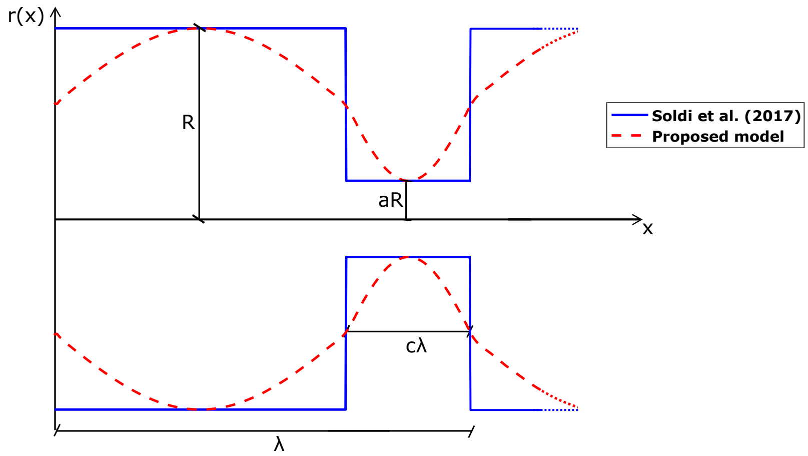

Figure 1: Pore geometry schemes for one wavelength of the constitutive models for a single capillary tube with periodic straight pore throats (blue) and periodic sinusoidal pore throats (red).

and also in the non-constrictive lengths of the pore (see Fig. 1). In this case, the pore radius along one wavelength λ of the tube can be expressed as:

$$r(x) = \begin{cases} \frac{R}{2}(1+a) + \frac{R}{2}(1-a)\sin\left(\frac{\pi}{\lambda(1-c)}x\right) & \text{if} \quad x \in [0, \lambda(1-c)), \\ \frac{R}{2}(1+a) + \frac{R}{2}(1-a)\sin\left(\frac{\pi}{\lambda c}[x-\lambda(1-2c)]\right) & \text{if} \quad x \in [\lambda(1-c), \lambda). \end{cases} \tag{2}$$

Note that, for $c = 0.5$, Eq. (2) is equivalent to the model of Guarracino et al. (2014) which considers the same length for the constrictive and non-constrictive fractions of the sinusoidal pore geometry. Hereafter, we will refer to this proposed model as the sinusoidal piecewise model.

Based on the above assumptions, expressions for the pore volume and volumetric water flow in a single pore can be obtained. By integrating the cross-sectional area over the length l of a capillary tube, the volume of a pore V_p (m^3) can be calculated as follows:

$$V_p = \int_0^l \pi r^2(x)dx = \pi R^2 l f_v(a,c), \tag{3}$$

where the dimensionless factor f_v varies between 0 and 1, and quantifies the reduction in the pore volume resulting from the presence of the pore throats. For the straight piecewise model, the expression of this factor yields (Soldi et al., 2017)

$$f_v(a,c) = a^2c + 1 - c, \tag{4}$$

while for the sinusoidal piecewise model, f_v is expressed as

$$f_v(a,c) = \frac{(1+a)^2}{4} + \frac{(1-a)^2}{8} + \frac{1}{\pi}(1-a^2)(1-2c). \tag{5}$$

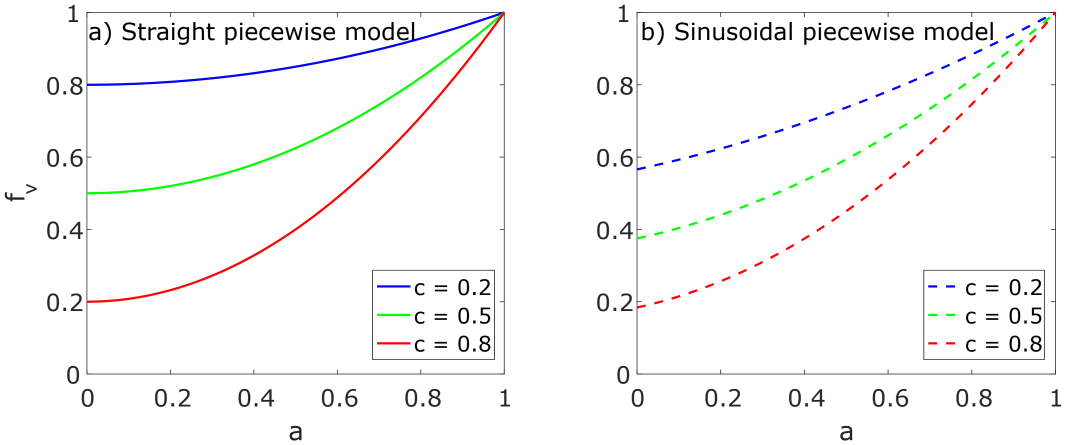

Figure 2: Dimensionless factor f_v as a function of the radial factor a for different constant values of parameter c: a) f_v factor of the straight piecewise model (Eq. (4)) and b) f_v factor of the sinusoidal piecewise model (Eq. (5)).

Note that for $a = 1$, $f_v = 1$ for both models and the expression obtained for Eq. (3) represents the volume of a capillary tube of constant radius R. Figure 2 shows the variation of f_v as a function of the radial factor a for different values of the length factor c. It can be observed that for a fixed value of a, f_v of the straight piecewise model varies in a wider range of values than the f_v factor of the sinusoidal piecewise model. Nevertheless, for both models it can be noticed that the presence of the pore throats affects significantly the volume of a pore.

Under the hypothesis of laminar flow and neglecting the convergence and divergence of the flow, the volumetric water flow q_p (m^3 s^{-1}) in the capillary tube represented by the geometry of the straight piecewise model can be approximated with (Bodurtha, 2003; Bousfield and Karles, 2004):

$$q_p = \frac{\rho g}{\mu}\left[\frac{1}{l}\int_0^l \frac{8}{\pi r^4(x)}dx\right]^{-1}\frac{\Delta h}{l} = \frac{\rho g}{\mu}\frac{\pi}{8}R^4 f_k(a,c)\frac{\Delta h}{l} \tag{6}$$

where ρ (kg m^{-3}) is the water density, g (m s^{-2}) gravity, μ (Pa s) water dynamic viscosity, Δh (m) the head drop across the tube and f_k a dimensionless factor given by (Soldi et al., 2017)

$$f_k(a,c) = \frac{a^4}{c + a^4(1-c)}. \tag{7}$$

This factor varies between 0 and 1, and quantifies the reduction in the volumetric flow rate due to the pore throats.

Assuming the same flow conditions and following the work of Guarracino et al. (2014), we calculate the volumetric flow for a capillary with sinusoidal piecewise geometry by considering an average radius ($R(1 + a)/2$) and an equivalent permeability (Reis and

Acock, 1994):

$$q_p = \frac{\rho g}{\mu}\left[\frac{1}{l}\int_0^l \frac{8}{\pi r^2(x)}dx\right]^{-1}\frac{R^2(1+a)^2}{4}\frac{\Delta h}{l} = \frac{\rho g}{\mu}\frac{\pi}{8}R^4 f_k(a,c)\frac{\Delta h}{l}, \tag{8}$$

from this equation, the factor f_k for the sinusoidal piecewise model is found and computed as follows

$$f_k(a,c) = \left[\frac{1}{l}\int_0^l \frac{dx}{r^2(x)}\right]^{-1}\frac{(1+a)^2}{4R^2}. \tag{9}$$

Substituting Eq. (2) in Eq. (9) and integrating, it yields

$$f_k(a,c) = \frac{a^{3/2}(1+a)}{2}\left\{(1-2c)\left[1-\frac{2}{\pi}\mathrm{tg}^{-1}\left(\frac{1-a}{2\sqrt{a}}\right)-\frac{4}{\pi}\frac{(1-a)\sqrt{a}}{(1+a)^2}\right]+2c\right\}^{-1}. \tag{10}$$

The exact expression of f_k given by Eq. (10) can be reduced to the following approximate expression

$$f_k(a,c) = \frac{a^{3/2}\pi(1+a)^3}{2\pi(1+a)^2-4(1-a)(1-2c)(1+\sqrt{a})^2}. \tag{11}$$

It is interesting to observe that the final expressions of Eqs. (6) and (8) are similar except for the factor f_k which differs with the geometry of each model. The variation of f_k as a function of the radial factor a is shown in Fig. 3 for both models, for different values of the length factor c. Note that the factor f_k controls the volumetric water flow in a pore and varies significantly with the geometry. While for the straight piecewise model f_k (Eq. (7)) drastically reduce the volumetric flow of the pore for decreasing values of parameter a (see Fig. 3a), for the sinusoidal piecewise model, f_k (Eq.(10)) produces gradual changes of the volumetric flow (Fig. 3b). Moreover, the f_k values for the sinusoidal piecewise model obtained by the exact and the approximate expressions (Eqs. (10) and (11)) are similar for all the range of parameter a values and for the different values of parameter c. Note also that if $a = 1$ then $f_k = 1$, and the expressions obtained for Eqs. (6) and (8) represent the volumetric flow of a capillary tube of constant radius R.

2.2 Hydraulic properties at REV scale

To derive the expressions of the hydraulic properties under total and partial saturation conditions, we consider a REV conceptualized as a circular cylinder of radius R_{REV} and length L. The pore structure of the REV is represented by a bundle of tortuous constrictive tubes with a fractal pore size distribution. We consider that the radius of the pores R varies from a minimum value R_{min} to a maximum value R_{max} and that the tortuosity τ (dimensionless) defined as $\tau = l/L$ is constant for all the bundle. Thus, τ can be understood as an effective macroscopic value for all the pores of the REV.

Based on the fractal theory, the cumulative size distribution of pores is assumed to obey the following law (Tyler and Wheatcraft, 1990; Guarracino et al., 2014; Soldi et al., 2017; Rembert et al., 2020):

$$N(R) = \left(\frac{R_{REV}}{R}\right)^D \tag{12}$$

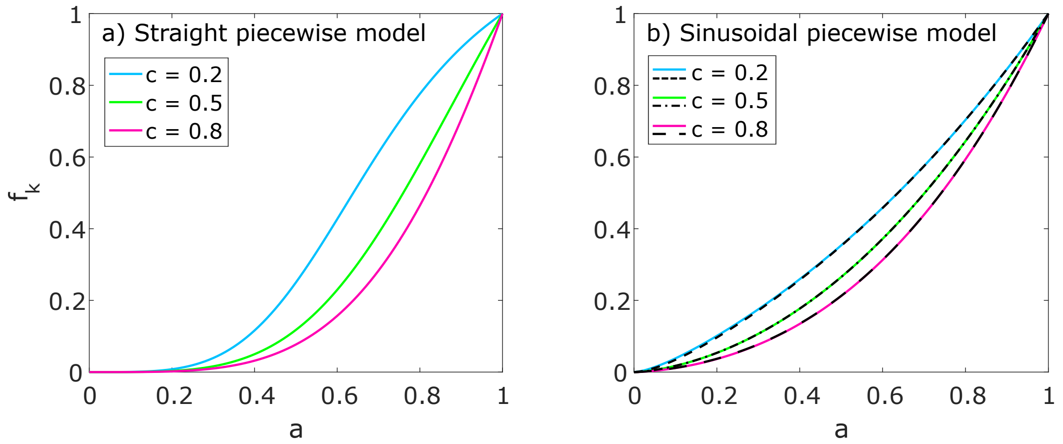

Figure 3: Dimensionless factor f_k as a function of the radial factor a for different constant values of parameter c: a) f_k factor of the straight piecewise model (Eq. (7)) and b) f_k factor of the sinusoidal piecewise model where the solid and dashed lines correspond to the exact and approximate expressions (Eqs. (10) and (11)), respectively.

where the radius of the pores remains in the range $0 < R_{min} \leq R \leq R_{max} < R_{REV}$ and D (dimensionless) is the fractal dimension of the pores. By using the Sierpinski carpet which is a classical fractal object, Tyler and Wheatcraft (1990) show that the fractal dimension D of Eq. (12) varies between 1 and 2 for different porous media. The number of pores whose radii are within the infinitesimal range R and $R + dR$ is obtained from Eq. (12) as follows:

$$-dN(R) = DR_{REV}^{D}R^{-D-1}dR \tag{13}$$

where the minus sign implies that the number of pores decreases when the radius of the pore increases (Yu et al., 2003; Thanh et al., 2019).

2.2.1 Porosity

The porosity of the REV ϕ (dimensionless) can be obtained straightforward from its definition as the quotient between the volume of pores and the volume of the REV as follows:

$$\phi = \frac{\int_{R_{min}}^{R_{max}} V_p(R)dN(R)}{\pi R_{REV}^2 L}. \tag{14}$$

Then, replacing Eq. (3) in Eq. (14), it yields:

$$\phi = f_v(a,c)\frac{D\tau}{R_{REV}^{2-D}(2-D)}\left[R_{max}^{2-D} - R_{min}^{2-D}\right] \tag{15}$$

being f_v the expression given by Eqs. (4) or (5) according to the geometry of the straight and sinusoidal piecewise models, respectively. Note that for $a = 1$, $f_v = 1$ for both models and the expression obtained for Eq. (15) represents the porosity of the REV considering non-constrictive tortuous tubes. It can also be noticed that, if $c = 0.5$, Eqs. (5) and (15) are consistent with the expressions of the model of Guarracino et al. (2014) when considering the case of non-tortuous capillaries (i.e. $\tau = 1$).

2.2.2 Permeability

We first calculate the volumetric flow rate q (m^3 s^{-1}) at REV scale in order to obtain the permeability of the REV. On the one hand, similar to the approach used by Yu et al. (2002, 2003), Soldi et al. (2017) and Chen et al. (2021), the flow q can be calculated by integrating all the pores volumetric flow rates given by Eq. (6) or (8) over the entire range of pore sizes:

$$q = \int_{R_{min}}^{R_{max}} q_p(R) dN(R) = \frac{\rho g}{\mu} \frac{\pi}{8} \frac{D R_{REV}^D}{(4-D)} f_k \frac{\Delta h}{l} \left[R_{max}^{4-D} - R_{min}^{4-D} \right]. \tag{16}$$

On the other hand, the volumetric flow through the REV can be expressed by Darcy's law for saturated porous media (Darcy, 1856) as:

$$q = \frac{\rho g}{\mu} k \pi R_{REV}^2 \frac{\Delta h}{L} \tag{17}$$

where k (m^2) is the permeability of the REV. Then, combining Eqs. (16) and (17) yields:

$$k = f_k(a, c) \frac{D R_{REV}^{D-2}}{8\tau(4-D)} \left[R_{max}^{4-D} - R_{min}^{4-D} \right] \tag{18}$$

where f_k is the expression given by Eq. (7) or (10) for the straight and sinusoidal piecewise models, respectively. Note that in the case of non-constrictive tubes (i.e., $a = 1$), $f_k = 1$ for both models and Eq. (18) describes the permeability of the REV with straight tortuous tubes. Also, note that if we consider non-tortuous capillaries, $\tau = 1$, and $c = 0.5$, Eqs. (10) and (18) are consistent with the expressions of the sinusoidal model of Guarracino et al. (2014).

2.2.3 Retention and Relative Permeability Curves

It is well-known that retention and relative permeability curves obtained from drainage and imbibition tests are different due to the hysteresis phenomenon. The effect of this phenomenon on those curves can be easily modeled with the pore geometries illustrated in Fig. 1 and described by Eqs. (1) and (2). We derive those curves expressions for the sinusoidal piecewise model similar to the approach used by Soldi et al. (2017) for the straight piecewise model and also by Guarracino et al. (2014) and by Chen et al. (2021).

The main drying effective saturation curve is obtained by considering that the REV is initially fully saturated and is drained by a pressure head h (m). This pressure can be related to a pore radius R_h by the following equation (Bear, 1998):

$$h = \frac{2T_s \cos(\beta)}{\rho g R_h}, \tag{19}$$

where T_s (N m^{-1}) is the surface tension of the water and β the contact angle. Note that Eq. (19) is the Young-Laplace equation which is valid for straight tubes. However, this equation can be used for the geometry described by Eq. (2) when considering that the pressure head value changes with the position of the wetting perimeter (Guarracino et al., 2014). The pore radius that corresponds to this position is the radius of the pore throat for both geometries, $R_h = aR$. Therefore, we assume that a tube becomes fully desaturated if its pore throat radius is greater than the radius R_h given by Eq. (19). It is then reasonable to also assume that pores within the range $R_{min} \leq R \leq R_h/a$ will remain fully saturated, and the main drying effective saturation curve S_e^d (dimensionless) can be expressed by:

$$S_e^d = \frac{\int_{R_{min}}^{R_h/a} V_p(R)dN(R)}{\int_{R_{min}}^{R_{max}} V_p(R)dN(R)} = \frac{(R_h/a)^{2-D} - R_{min}^{2-D}}{{R_{max}}^{2-D} - R_{min}^{2-D}}. \tag{20}$$

The S_e^d curve can also be expressed as a function of the pressure head by substituting Eq. (19) in (20):

$$S_e^d(h) = \begin{cases} 1 & \text{if} \quad h \leq \frac{h_{min}}{a} \\ \frac{(ha)^{D-2} - h_{max}^{D-2}}{h_{min}^{D-2} - h_{max}^{D-2}} & \text{if} \quad \frac{h_{min}}{a} < h < \frac{h_{max}}{a} \\ 0 & \text{if} \quad h \geq \frac{h_{max}}{a}, \end{cases} \tag{21}$$

where

$$h_{min} = \frac{2T_s \cos(\beta)}{\rho g R_{max}} \qquad \text{and} \qquad h_{max} = \frac{2T_s \cos(\beta)}{\rho g R_{min}}, \tag{22}$$

h_{min} and h_{max} are the minimum and maximum pressure heads defined by R_{max} and R_{min}, respectively.

Similarly, for an imbibition experiment, the main wetting effective saturation curve S_e^w (dimensionless) can be obtained assuming that the REV is initially dry and it is flooded with a pressure h. Only the tubes whose radius R is smaller than R_h will be fully saturated in this case and the S_e^w curve can be computed as:

$$S_e^w(h) = \begin{cases} 1 & \text{if} \quad h \leq h_{min} \\ \frac{h^{D-2} - h_{max}^{D-2}}{h_{min}^{D-2} - h_{max}^{D-2}} & \text{if} \quad h_{min} < h < h_{max} \\ 0 & \text{if} \quad h \geq h_{max}. \end{cases} \tag{23}$$

To obtain the relative permeability curves, we consider the same hypotheses and neglect film flow on surfaces of the tubes. During a drainage experiment, the pores that contribute to the total volumetric flow through the REV q (m^{3}s^{-1}) are those that remain saturated ($R_{min} \leq R \leq R_h/a$). Then, q can be obtained by integrating the individual volumetric flow rates q_p given by Eq. (6) or (8) as follows (similar to Yu et al. (2002) and Yu (2008)):

$$q = \int_{R_{min}}^{R_h/a} q_p(R)dN(R). \tag{24}$$

Based on Buckingham-Darcy law for unsaturated water flow (Buckingham, 1907), the volumetric flow through the REV can be expressed by:

$$q = \frac{\rho g}{\mu} k k_{rel} \pi R_{REV}^2 \frac{\Delta h}{L} \tag{25}$$

where k_{rel} (dimensionless) is the relative permeability. Combining Eqs. (24) and (25), an expression for the main drying relative permeability curve k_{rel}^d can be obtained:

$$k_{rel}^d(R_h) = \frac{(R_h/a)^{4-D} - R_{min}^{4-D}}{{R_{max}}^{4-D} - R_{min}^{4-D}}. \tag{26}$$

Using Eq. (19) we can express Eq. (26) as a function of the pressure head:

$$k_{rel}^d(h) = \begin{cases} 1 & \text{if} \quad h \leq \frac{h_{min}}{a} \\ \frac{(ha)^{D-4} - h_{max}^{D-4}}{h_{min}^{D-4} - h_{max}^{D-4}} & \text{if} \quad \frac{h_{min}}{a} < h < \frac{h_{max}}{a} \\ 0 & \text{if} \quad h \geq \frac{h_{max}}{a}. \end{cases} \tag{27}$$

Otherwise, for an imbibition experiment, the main wetting relative permeability curve k_{rel}^w can be derived similarly by integrating Eq. (24) over the range of saturated pores ($R_{min} \leq R \leq R_h$):

$$k_{rel}^w(h) = \begin{cases} 1 & \text{if} \quad h \leq h_{min} \\ \frac{h^{D-4} - h_{max}^{D-4}}{h_{min}^{D-4} - h_{max}^{D-4}} & \text{if} \quad h_{min} < h < h_{max} \\ 0 & \text{if} \quad h \geq h_{max}. \end{cases} \tag{28}$$

Note that Eqs. (21), (23), (27) and (28) can be used to calculate the main drying and wetting curves of the hysteretic cycle observed in the effective saturation and relative permeability. These expressions have analytical closed forms with only four independent parameters with geometrical or physical meaning (a, D, h_{min} and h_{max}). It can also be noted that these relative properties of the medium (S_e and k_{rel}) have the same expressions for both the sinusoidal and straight piecewise models and are independent of the length factor c of the geometries. Therefore, variations of the pore geometry affect only the expressions of the porosity ϕ and permeability k of the medium while no effects are present in the relative hydraulic properties.

2.2.4 Relationships between the hydraulic properties

In this section, we derive relationships between the macroscopic hydraulic properties of the porous medium, porosity and permeability, and effective saturation and relative permeability following the approach used by Soldi et al. (2017).

In order to obtain a relationship between permeability k and porosity ϕ, we assume that $R_{min} \ll R_{max}$ and then the terms R_{min}^{2-D} and R_{min}^{4-D} can be considered negligible in Eqs. (15) and (18). Indeed, for most porous media, the ratio between the R_{min} and R_{max} values is smaller than 10^{-2} (e.g. Yu and Li, 2001). Under this assumption and combining the resulting expressions, we obtain the following equation:

$$k(\phi) = \frac{DR_{REV}^2}{8\tau(4-D)} f_k(a,c) \left(\frac{2-D}{D\tau f_v(a,c)} \right)^{\frac{4-D}{2-D}} \phi^{\frac{4-D}{2-D}}. \tag{29}$$

This equation allows to estimate the permeability as function of porosity while also depending on the pore geometry factors (a and c) through the factors f_v and f_k, the fractal dimension, the tortuosity and the radius of the REV. Given the similarity of the k and ϕ expressions of the sinusoidal and straight piecewise models, the $k(\phi)$ relationship can be used for both models by taking into account the respective f_v and f_k factors of each model. Note that, in the limit case of $D = 1$, Eq. (29) becomes similar to the Kozeny-Carman equation (Kozeny, 1927; Carman, 1937). The relative permeability k_{rel} and effective saturation S_e are estimated as function of a pore radius R_h by Eqs. (20) and (26). Nevertheless, these equations can be combined to obtain a relationship between k_{rel} and S_e for both the drying and imbibition experiments and yields:

$$k_{rel}(S_e) = \frac{\left[S_e\left(\alpha^{D-2}-1\right)+1\right]^{\frac{4-D}{2-D}} - 1}{\alpha^{D-4}-1} \tag{30}$$

where $\alpha = R_{min}/R_{max}$. Note that Eq. (30) has the same expression for both the straight and sinusoidal piecewise models. It is also interesting to remark that, when k_{rel} is expressed in terms of S_e, the function obtained is non–hysteretic. This means that the relationship between these two relative hydraulic properties is unique for the drying and imbibition which is in agreement with a number of experimental data (e.g. Topp and Miller, 1966; Van Genuchten, 1980; Mualem, 1986).

The model presented in this section is derived in the framework of capillary tube models. There are two characteristic limitations that affect the models based on this framework (e.g. Chen et al. 2021). The first limitation is that the lateral connectivity in between the pores is not considered in the capillary system. There are no points of intersection between capillaries and all of them run parallel with the same orientation. The second limitation is that the hysteresis phenomenon on hydraulic properties cannot be described by classical capillary tube models since the assumption of capillaries with constant aperture is a very strong idealization for a real pore channel. Nevertheless, the proposed model assumes irregularities in the pores which allows us to include this phenomenon in effective saturation and relative permeability.

3 Sensitivity analysis of the geometrical parameters

In this section, a sensitivity analysis of the geometrical parameters of the models is addressed to study the effect of the pore structure on the hydraulic properties. Hence, we perform a parametric analysis of Eqs. (15) and (18) to estimate the porosity and permeability of the REV using Eqs. (4) and (7), and (5) and (10) to calculate the f_v and f_k factors for the straight and sinusoidal piecewise models, respectively. We test the influence of the radial factor a that controls the pore throats amplitude and the length factor c which controls the pore throats length. The estimates of ϕ and k also depend on other characteristics of the porous medium, for both models, the following values are then considered: $R_{REV} = 5$ cm, $D = 1.5$, $\tau = 1.4$, $R_{min} = 1.5 \times 10^{-4}$ mm and $R_{max} = 1.5$ mm.

Figure 4 summarizes this analysis and shows how the pore geometry modifies the macroscopic values of the properties. For low values of parameter c, the porosity estimated by the straight piecewise model is higher than the corresponding to the sinusoidal piecewise model (see Fig. 4a and 4b). This difference in the porosity is schematically represented by the grey area in Figure 4c-e where the pore geometry is shown for different values of parameters a and c. It can be seen that the area of the constrictive fraction of the pore is greater for the sinusoidal piecewise model than for the straight piecewise model. However, this excess area is smaller than the excess area of the straight piecewise model in the non-constrictive fraction of the pore. In these cases, the effect of geometry on porosity causes changes in this property of 5-10% approximately between the models. Figure 4f-g show the estimates of permeability which present different patterns of variation for the models. Note that for high values of parameter c, the permeability estimates of the straight piecewise model decrease faster than the estimates of the sinusoidal piecewise model when decreasing parameter a. However, the greatest differences between the permeability estimates are associated to low values of parameter c (short pore throats) over the entire range of parameter a. It can also be noticed that both models can estimate media with high permeability and high porosity, and also with low permeability and high porosity. Therefore, these models are able to represent a wide range of porous media. Although the straight piecewise model might consider a more simple pore shape structure, the sinusoidal piecewise model's geometry has the advantage of being more similar to a real porous media since it presents no abrupt changes between the constrictive and non-constrictive fractions of the pore.

The hysteresis phenomenon caused by the irregularities in the pore structure is explicitly observed in the effective saturation (S_e) and relative permeability (k_{rel}) when expressed as functions of the pressure head (Eqs. (21), (23), (27) and (28)). It is important to remark that the main drying and wetting curves of S_e and k_{rel} obtained for the straight and sinusoidal piecewise models have the same analytical expressions. Therefore, under the hypotheses of these models, considering the pore shape as straight or sinusoidal piecewise has no influence on S_e and k_{rel}. However, the expressions of S_e and k_{rel} depend on the geometrical parameter a while they are independent of parameter c. For this reason, we only test the effect of a that controls the amplitude of the pore throats geometry. We consider the same reference values used for the previous sensitivity analysis for parameters D, R_{min} and R_{max}. Figure 5 shows the effect of the radial factor a in the curves of the hydraulic properties S_e and k_{rel}. It can be observed that the influence of this parameter is significant in the main drying curves of S_e and k_{rel} for the entire range of pressure head values. Nevertheless, no effect of this parameter is observed on the main wetting curves of both properties since Eqs. (23) and (28) are independent of a. Note that the hysteresis cycle for S_e and k_{rel} increases for low values of a since the limit pressure head values (h_{min}/a and h_{max}/a) of the main drying curves (Eqs. (21) and (27)) shift to higher values, which increases the distance between the main drying and wetting curves. Nonetheless, the two main curves of S_e and k_{rel} tend to reduce their distance when a tends toward 1, as it can be expected since this limit case represents a tube of constant radius and thus no hysteretic phenomenon is observed in straight capillaries.

From this parametric analysis, we can conclude that the presence of constrictivities defined by parameters a and c leads to differences in the estimates of ϕ and k, while only parameter a affects the estimates of S_e and k_{rel}. The most significant variations on the ϕ and k estimates are reached for low values of parameter c. Furthermore, an interesting result is that both models allows to represent porous media with high porosity and low permeability such as clays which cannot be properly represented with straight capillary models. The analysis of the relative hydraulic properties shows that the estimates of the main drying S_e and k_{rel} curves are highly sensitive to parameter a and that the greatest differences between the the main drying and wetting S_e and k_{rel} curves are observed for decreasing values of a.

4 Comparison with experimental data

In the present section, we test the ability of the proposed model to reproduce available measured data from the research literature. These data sets consist of measured permeability–porosity, hydraulic conductivity-pressure head, water content-pressure head and hysteretic water content–pressure values for different soil textures.

4.1 Water content and hydraulic conductivity laboratory data

In order to test the estimates of the proposed model, we selected three experimental data sets from different soil textures: a coarse granular material named GW Substrate from Stanić et al. (2020a), a well graded sand and a silty clay sand named Okcheon 2 and Seochang, respectively, from Oh et al. (2015). These data series consist of water content and hydraulic conductivity values as a function of pressure head which were measured during drainage experiments. As it is well known, hydraulic conductivity K (mD) and permeability k are related through $K = k\rho g/\mu$, while water content θ (dimensionless) is related to saturation S through the porosity ϕ of the medium. The test of the sinusoidal piecewise model relies on fitting Eqs. (15) and (21), and Eqs. (18) and (27) for the water content and the hydraulic conductivity data sets, respectively.

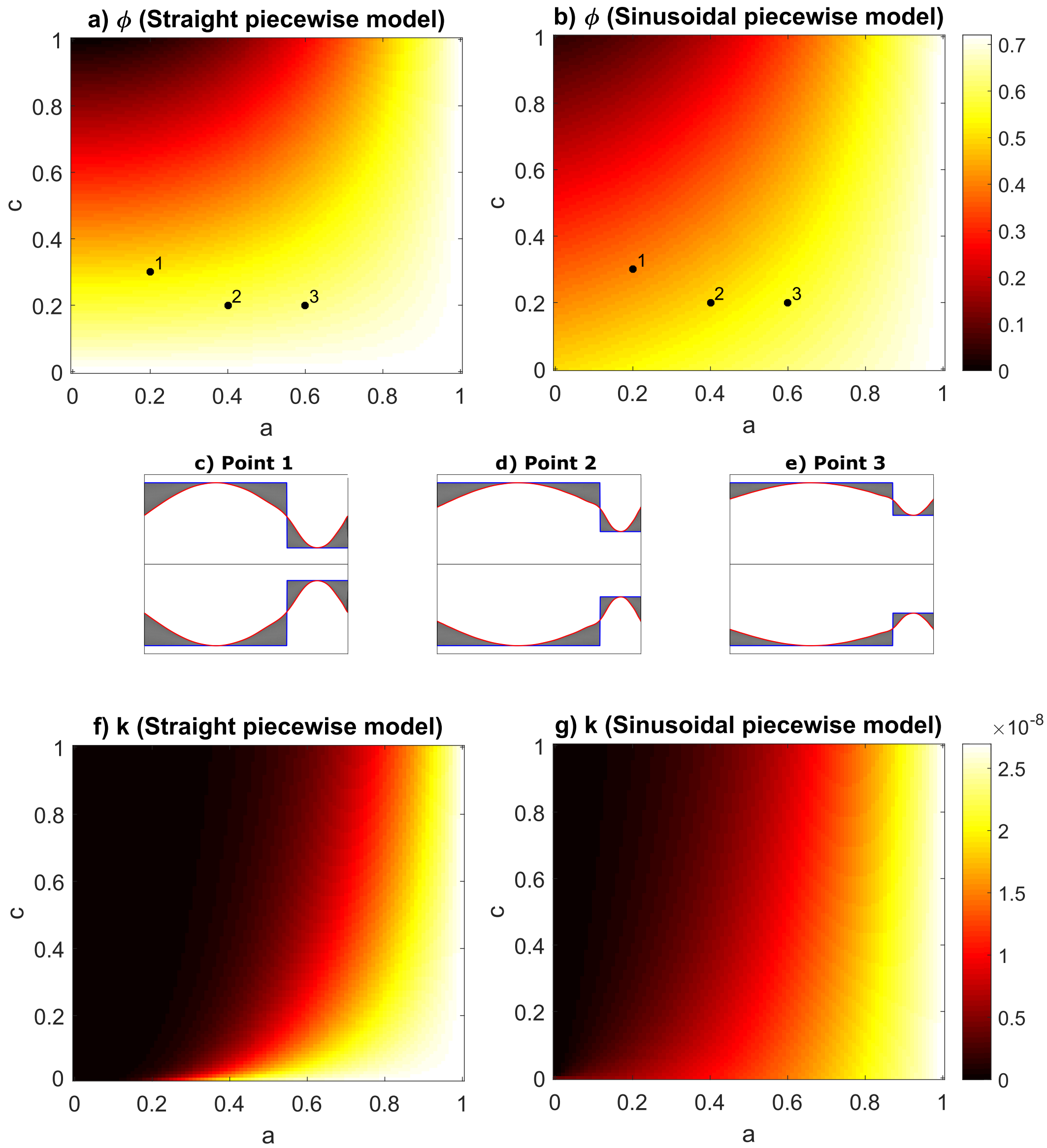

Figure 4: Parametric analysis of the porosity and permeability as functions of the radial and length factors, a and c, respectively: a) and f) for the straight piecewise model (Soldi et al., 2017), b) and g) for the sinusoidal piecewise model. Note that fixed values of the remaining parameters were considered in each case. Figs. c, d and e) show schematic representations of the pore structure for $a = 0.2$ and $c = 0.3$, $a = 0.4$ and $c = 0.2$, and $a = 0.6$ and $c = 0.2$, respectively, for the straight and sinusoidal piecewise models. The grey area indicates the difference in the pore volume between the models.

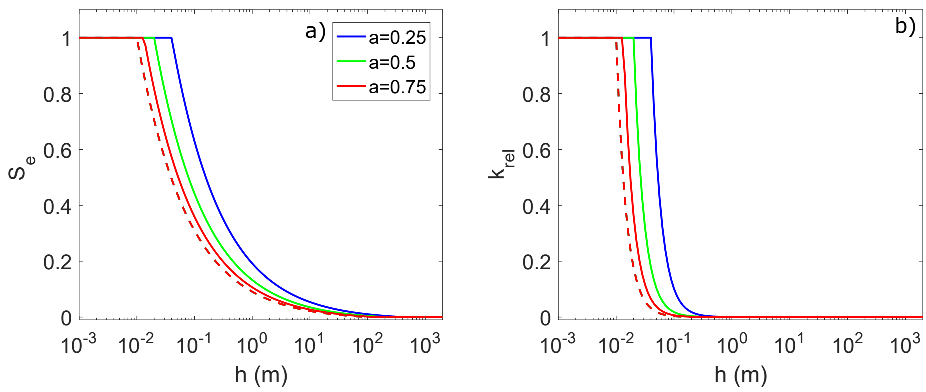

Figure 5: Parametric analysis of the relative properties: a) effective saturation and b) relative permeability, for drainage (solid lines) and imbibition (dashed lines), sensitivity to the radial factor a. In each case, fixed values of the remaining parameters are considered.

Table 1: Values of the fitted parameters (D, τ, a and c) for the water content and hydraulic conductivity curves using the sinusoidal piecewise model, and the corresponding values of h_{min} and h_{max}.

Soil type	Sinusoidal piecewise model parameters					
	D	τ	a	c	h_{min} (m)	h_{max} (m)
Okcheon 2	1.729	1.257	0.35	0.78	0.297	5×10^4
Seochang	1.711	1.296	0.41	0.85	0.367	10×10^3
GW substrate	1.601	1.198	0.58	0.70	0.154	50×10^4

Figure 6 illustrates the fit between the sinusoidal piecewise model and the experimental data sets. Table 1 lists the fitted parameters (D, τ, a and c). These parameters have been estimated by an exhaustive search method by minimizing the weighted normalized error between calculated and experimental data values for both the water content and hydraulic conductivity curves simultaneously. This model also requires specifying the minimum and maximum pressure heads which are determined by trial-and-error method, as well as the REV radius that is taken from Stanić et al. (2020a) and Oh et al. (2015) in order to reduce the number of the fitting parameters. Note that the sinusoidal piecewise model fits fairly well the data and can estimate the order of magnitude of the hydraulic properties for the different soils. It is interesting to remark that the model is able to reproduce the behaviour of the data with only one set of parameters for both hydraulic properties simultaneously.

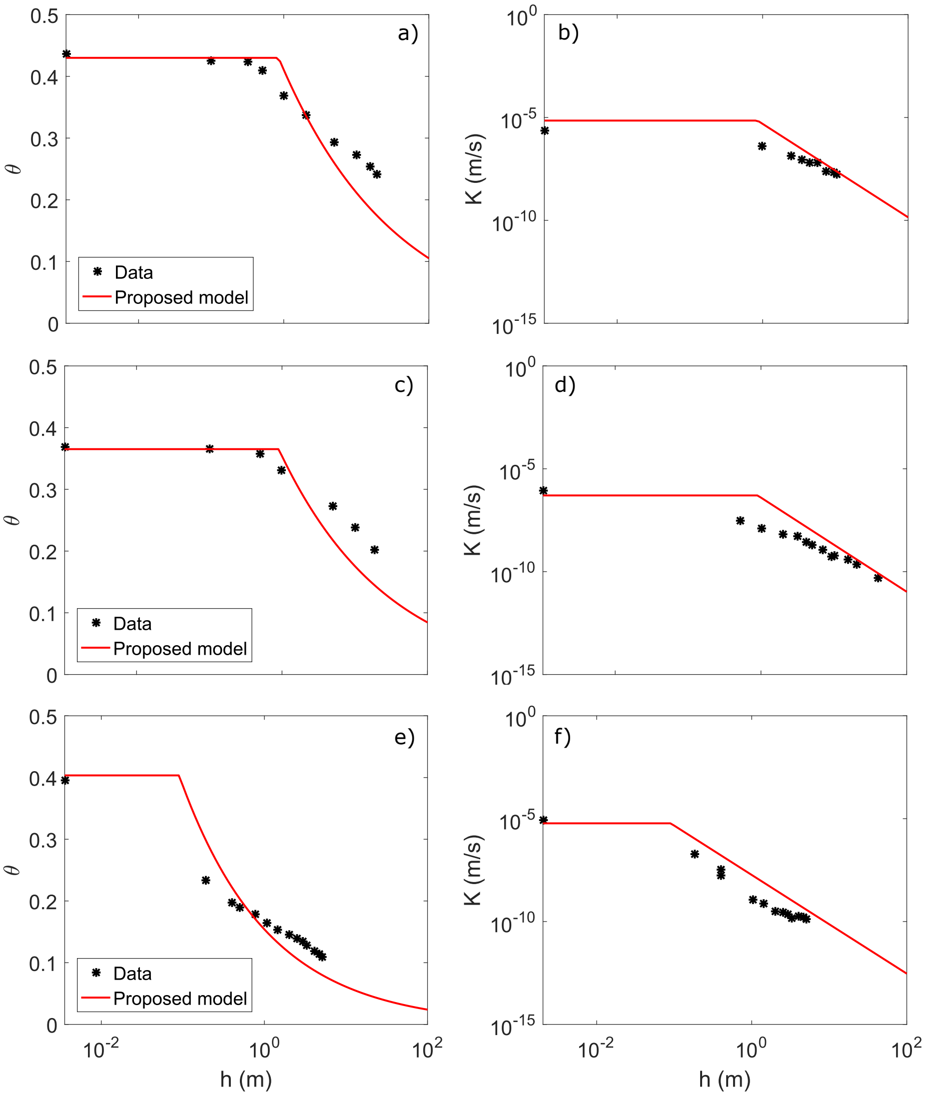

Figure 6: Comparison of the water content and hydraulic conductivity curves from the sinusoidal piecewise model with experimental data sets for a drainage experiment: a-b) okcheon 2, c-d) seochang (data from Oh et al., 2015) and e-f) GW substrate (data from Stanić et al., 2020a).

4.2 Permeability-porosity relationship

In Section 2.2.4 we derived a relationship between permeability and porosity (Eq. (29)) that depends on the geometry of the model through the factors $f_v(a, c)$ and $f_k(a, c)$. We selected experimental data series from two different types of clays (an illite and a kaolinite) from Mesri and Olson (1971) to test the estimates of this equation. These estimates are calculated for both the sinusoidal and straight piecewise models using their respective relationship with the factors f_v and f_k of each model (Eqs. (5) and (10), and (4) and (7), respectively). In addition, we compare these relationships with the most classical equation to represent permeability-porosity data, the Kozeny-Carman equation (Kozeny, 1927; Carman, 1937), that can be expressed as follows:

$$k = \alpha_{KC} \frac{\phi^3}{(1-\phi)^2} \tag{31}$$

being α_{KC} a parameter that depends on the specific internal surface area, the tortuosity and an empirical geometrical parameter.

The model parameters have been estimated using an exhaustive search method, which is a simple and very robust technique. To apply this method, we use the admissible ranges for each parameter: $0 < a, c < 1$ and $1 < D < 2$, and we consider $1 < \tau < 2$ as representative values of tortuosity in a sedimentary porous medium. The exhaustive search method computes the error between data and predicted values for all possible combinations of the model parameters values and selects the ones that minimize the root-mean-square deviation (RMSD) between the calculated and experimentally measured values. Figure 7 shows the fits of the proposed relationships for both piecewise models (Eq. (29)) and the Kozeny-Carman equation (Eq. (31)). Table 2 lists the fitted parameters for the equations as well as their respective RMSD. Note that for Eq. (29), we fit parameters D, τ, a and c for the sinusoidal and straight piecewise models. Eq. (29) also requires a R_{REV} value for which we consider the value from Mesri and Olson (1971), $R_{REV} = 5$ cm. It is important to remark that the values of parameters D and τ are the same for both models since they describe the same soil. Hence, we are able to highlight the effects of geometry through the fitting of the radial a and length c factors of each model. It can be observed that the proposed relationships fit fairly well both data sets for the entire range of porosities (Fig. 7). The geometry of the pores given by the fitted parameters presents smooth variations between the constrictive and non-constrictive fractions since the high values of c and a represent that the length of the pore throat is large and that the pore throat radius varies slightly from the pore radius. The comparison with the Kozeny-Carman equation shows that the proposed relationships provide much more better estimates. Indeed, it can be noted that the difference between the RMSD of the sinusoidal and straight piecewise models is not significant, and that they are smaller than the ones obtained from the fit of the Kozeny-Carman equation for both data sets.

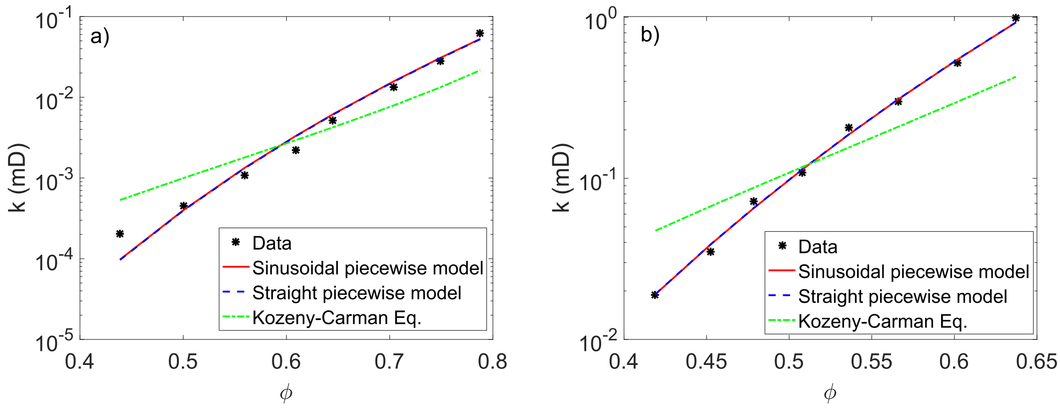

Figure 7: Comparison among the estimates of Eq. (29) for the sinusoidal and straight piecewise models, the Kozeny-Carman equation and experimental data sets of permeability–porosity for: a) illite and b) kaolinite (data from Mesri and Olson (1971)).

Table 2: Values of the fitted parameters (D, τ, a and c) and the RMSD for Eq. (29) when considering the sinusoidal and straight piecewise models, and for the Kozeny-Carman equation (Eq. (31)).

Model parameters	Soil type	
	Illite	Kaolinite
Sinusoidal piecewise model		
D	1.795	1.758
τ	1.46	1.60
a	0.92	0.90
c	0.91	0.79
RMSD	0.1421	0.0301
Straight piecewise model (Soldi et al., 2017)		
D	1.795	1.758
τ	1.46	1.60
a	0.90	0.89
c	0.60	0.70
RMSD	0.1422	0.0303
Kozeny-Carman (Eq. (31))		
α_{KC}	0.002	0.217
RMSD	0.3032	0.2447

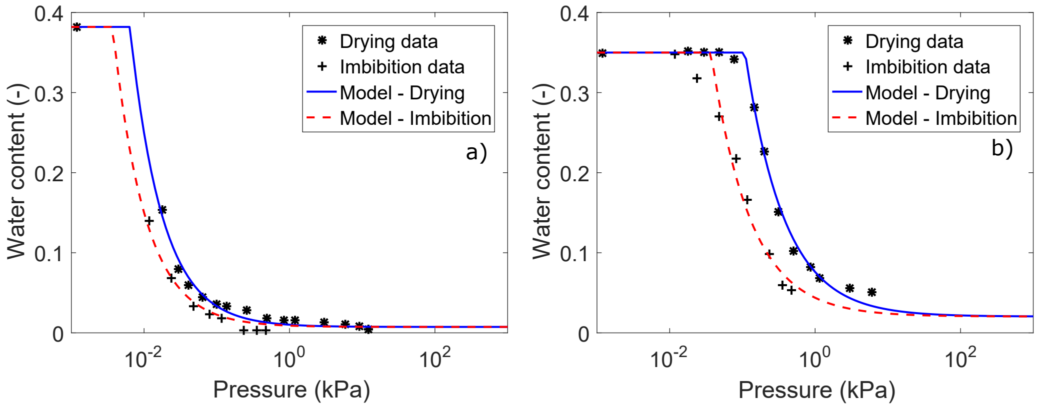

Figure 8: Comparison of the main drying and wetting water content curves with experimental data sets: a) gravelly sand and b) medium sand (data from Yang et al. (2004)).

4.3 Hysteresis in the water content

The performance of the model to describe the hysteresis phenomenon on the relative hydraulic property is tested by using available data from the literature. These experimental data consist of two sets of measured water content and pressure values for two different sands from Yang et al. (2004). Eqs. (21) and (23) are used to estimate the main drying and wetting effective saturation curves which are then converted to water content values in order to compare with the data.

Figure 8 shows the main drying and wetting water content curves fitted with the proposed model for the two sands. The best-fitted parameters (D, a, h_{min} and h_{max}) are listed in Table 3 as well as the RMSD values for each sand. Note that the hysteretic behavior of the water content can be satisfactorily reproduced by the model (see Fig. 8). It can also be observed that for the gravelly sand the distance between the main drying and wetting curves is smaller than for the main curves of the medium sand. This result can be related to the size distribution and geometry of the pores which are represented in the model by the fractal dimension D and the radial factor a. Comparing the values of D and a shown in Table 3, note that the lowest value of D is obtained for the gravelly sand which can be expected since low fractal dimensions values are associated to coarse textured soils and the high values of the radial factor a represent less constrictive pores. In fact, higher values of a represent pores with greater volume and thus a soil with higher porosity. From the measured porosity values by Yang et al. (2004), it can be noted that these geometrical results from the estimates of the models are consistent with the experimental measures that evidence the higher porosity of the gravelly sand (38.2%) over the medium sand (35%).

Table 3: Values of the fitted parameters (D, a, h_{min} and h_{max}) for the water content main drying and wetting curves, and the corresponding RMSD.

Soil type	Models parameters				
	D	a	h_{min} (kPa)	h_{max} (kPa)	RMSD
Medium sand	1.19	0.34	0.037	910	0.0264
Gravelly sand	1.03	0.58	0.004	70	0.0126

5 Discussion and Conclusions

The present study is focused on the analysis of pore geometry effects in the hydraulic properties of porous media. We compare two constitutive analytical models based on physical and geometrical concepts which include the hysteresis phenomenon in the hydraulic properties by considering irregularities in the structure of the pores. The straight piecewise model (Soldi et al., 2017) assumes that the pore space is represented by a bundle of tortuous capillary tubes with straight periodic reductions in the pore radius, while the sinusoidal piecewise model developed in this study represents the pore space as a bundle of sinusoidal tortuous capillaries with varying aperture. Based on a fractal distribution of pore sizes and upscaling procedures at pore and REV scales, analytical closed-form expressions are obtained for porosity, permeability, effective saturation and relative permeability. These expressions depend on independent parameters: a, c, D, τ, R_{min}, R_{max} and R_{REV}, all of them with a specific physical or geometrical meaning.

Capillary tube models have been proposed for over 100 years and have provided a valuable insight into the characterization of flow and hydraulic properties of porous media (Cai et al., 2022). Some of the most well-known models based on this approach of capillary tubes are the van Genuchten and the Brooks and Corey models. However, since these models assume cylindrical tubes of constant radii, they cannot describe the hysteresis phenomenon present in the hydraulic properties. The hysteresis has been easily included in the proposed model due to its pore geometry with variable radius, enhancing the hypothesis of pore throat effects as the possible cause of that phenomenon. Nevertheless, other effects (such as contact angle, wettability or network effects) can also contribute or justify hysteresis in porous media (Jury et al., 1991; Blunt et al., 2002; Spiteri et al., 2008). Note that when considering non-constrictive tubes ($a = 1$) and $R_{max} \gg R_{min}$, it can be shown that the effective saturation and relative permeability expressions are similar to the ones of Brooks and Corey, and that the proposed permeability-porosity relationship is similar to that of Kozeny-Carman. Moreover, the presence of pore throats in the geometry allows the proposed model to describe media with high porosity and low permeability which cannot be properly represented with straight capillary tube models. Finally, if the constrictive and non-constrictive fractions of the pore have the same length ($c = 0.5$), the proposed model is also consistent with the model derived by Guarracino et al. (2014) when considering the case of non-tortuous tubes ($\tau = 1$).

The pore geometry modifies the macroscopic properties, porosity and permeability, through the factors $f_v(a,c)$ and $f_k(a,c)$ whose expressions differ for the sinusoidal and straight piecewise models. The influence of the model parameters a and c on the estimates of porosity and permeability has been tested by a sensitivity analysis. The results show that the most significant differences between the estimates of the models are obtained for low values of the length factor c over the entire range of the radial factor a values for both properties.

The estimates of effective saturation S_e and relative permeability k_{rel} have also been studied by a parametric analysis. It is important to remark that the main S_e and k_{rel} drying and wetting curves have the same analytical expressions for both the sinusoidal and straight piecewise models. The expressions of those hydraulic properties are independent of c while depending on a that define the irregularities in the pore geometry. The results of the analysis show that the radial factor a controls the shape of the hysteretic loop (the distance between the drainage and imbibition curves), and in the limit case of $a = 1$ (straight tubes), the hysteresis disappears from the main curves as it will be expected.

The sinusoidal piecewise model is compared with experimental data from different soil textures. The estimates of hydraulic conductivity and water content as a function of the pressure head fit fairly well the data. In fact, the model is able to reproduce the behaviour of the data from the fitting of one set of parameters for both hydraulic properties simultaneously.

The models studied in this work provide relationships that estimate permeability as a function of porosity. The comparison with experimental data shows that these relationships are satisfactorily able to reproduce the measured data over the entire range of porosities. Moreover, the agreements obtained for the sinusoidal and straight piecewise models are significantly better than the fit provided by the Kozeny-Carman equation.

The performance of the model to describe the hysteresis phenomenon present in the relative hydraulic properties is tested with experimental data sets of volumetric water content and pressure for drainage and imbibition experiments. The hysteretic behavior can be fairly reproduced by the model for two different sand textures. The comparison of the hysteretic loops for the two sands shows that the distance between the main drying and wetting curves is smaller for the finest texture. This result is consistent with the fitted values of the model parameters (a and D) which are related to the pore-size distribution and geometry, and with the experimental measures of the soils properties from Yang et al. (2004).

The comparison between the sinusoidal and straight piecewise models shows that porosity and permeability are the most sensitive hydraulic properties to the pore geometry changes. Nevertheless, the relative properties, effective saturation and relative permeability, present no variations for the same geometrical parameters of the models. The sinusoidal piecewise model represents an improvement over the straight piecewise model since its geometry is more similar to a real porous media due to the smooth changes between the constrictive and non-constrictive lengths of the pore. Moreover, the sinusoidal piecewise model is a step forward in the geometry of capillary tube models whose key feature is to know the ratio between the pore throat radius and the pore radius. This ratio is directly related to the radial factor a, and for a better characterization of a porous medium, it can be experimentally measured by applying the mercury injection method (Gao and Hu, 2013). Nonetheless, both studied models can be a valuable starting point to describe other physical phenomena that require hydraulic description at pore scale or accounting for the hysteresis phenomenon in the hydraulic properties and, therefore, enhancing the possibility to a better understand of the processes that occur in the vadose zone.

6 Notation List

Declarations

Funding: Not applicable.
Conflicts of interest/Competing interests: The authors declare that they have no conflict of interest.
Availability of data and material: Not applicable. No original data, everything has been published before.
Code availability: Not applicable.
Authors' contributions: Conceptualization: MS, LG, DJ; Methodology: MS, LG, DJ; Writing-original draft preparation: MS, LG, DJ; Writing-review and editing: MS, LG, DJ; Investigation: MS, LG, DJ; Supervision: LG, DJ.

References

Bear, J., 1998. Dynamics of fluids in porous media. Dover Publications, Inc., Mineola, N.Y.

Blunt, M.J., Jackson, M.D., Piri, M., Valvatne, P.H., 2002. Detailed physics, predictive capabilities and macroscopic consequences for pore-network models of multiphase flow. Advances in Water Resources 25, 1069–1089.

Bodurtha, P., 2003. Novel techniques for investigating the permeation properties of environmentally-friendly paper coatings: The influence of structural anisotropy on fluid permeation in porous media. University of Plymouth.

Bousfield, D.W., Karles, G., 2004. Penetration into three-dimensional complex porous structures. Journal of colloid and interface science 270, 396–405.

Brooks, R.H., Corey, A.T., 1964. Hydraulic properties of porous media and their relation to drainage design. Transactions of the ASAE 7, 26–0028.

Bryant, S., Blunt, M., 1992. Prediction of relative permeability in simple porous media. Physical review A 46, 2004.

Buckingham, E., 1907. Studies on the movement of soil moisture. US Dept. Agic. Bur. Soils Bull. 38.

Burdine, N.T., 1953. Relative permeability calculations from pore size distribution data. Journal of Petroleum Technology 5, 71–78.

Cai, J., Chen, Y., Liu, Y., Li, S., Sun, C., 2022. Capillary imbibition and flow of wetting liquid in irregular capillaries: A 100-year review. Advances in Colloid and Interface Science , 102654.

Carman, P.C., 1937. Fluid flow through granular beds. Trans. Inst. Chem. Eng. 15, 150–166.

Chen, K., Liang, F., Wang, C., 2021. A fractal hydraulic model for water retention and hydraulic conductivity considering adsorption and capillarity. Journal of Hydrology 602, 126763.

Darcy, H., 1856. Exposition et application des principes à suivre et des formules à employer dans les questions de distribution d'eau. Les fontaines publiques de la ville de Dijon, Eds. Victor Dalmont, Paris 1856.

Dong, H., Blunt, M.J., 2009. Pore-network extraction from micro-computerized-tomography images. Physical review E 80, 036307.

Gao, Z., Hu, Q., 2013. Estimating permeability using median pore-throat radius obtained from mercury intrusion porosimetry. Journal of Geophysics and Engineering 10, 025014.

Guarracino, L., Rötting, T., Carrera, J., 2014. A fractal model to describe the evolution of multiphase flow properties during mineral dissolution. Advances in water resources 67, 78–86.

Joekar-Niasar, V., Prodanović, M., Wildenschild, D., Hassanizadeh, S.M., 2010. Network model investigation of interfacial area, capillary pressure and saturation relationships in granular porous media. Water Resources Research 46.

Jougnot, D., Mendieta, A., Leroy, P., Maineult, A., 2019. Exploring the effect of the pore size distribution on the streaming potential generation in saturated porous media, insight from pore network simulations. Journal of Geophysical Research: Solid Earth 124, 5315–5335.

Jury, W.A., Gardner, W.R., Gardner, W.H., 1991. Soil physics. John Wiley & Sons, Inc. New York .

Kozeny, J., 1927. Uber kapillare leitung der wasser in boden. Royal Academy of Science, Vienna, Proc. Class I 136, 271–306.

Lindquist, W.B., Venkatarangan, A., Dunsmuir, J., Wong, T.f., 2000. Pore and throat size distributions measured from synchrotron x-ray tomographic images of fontainebleau sandstones. Journal of Geophysical Research: Solid Earth 105, 21509–21527.

Man, H.N., Jing, X.D., 1999. Network modelling of wettability and pore geometry effects on electrical resistivity and capillary pressure. Journal of Petroleum Science and Engineering 24, 255–267.

Mesri, G., Olson, R.E., 1971. Mechanisms controlling the permeability of clays. Clays and Clay minerals 19, 151–158.

Moebius, F., Or, D., 2012. Interfacial jumps and pressure bursts during fluid displacement in interacting irregular capillaries. Journal of colloid and interface science 377, 406–415.

Mualem, Y., 1976a. A catalog of the hydraulic properties of unsaturated soils. Research Project 442, Technion-Israel Inst. Technol., Haifa , 100p.

Mualem, Y., 1976b. A new model for predicting the hydraulic conductivity of unsaturated porous media. Water resources research 12, 513–522.

Mualem, Y., 1986. Hydraulic conductivity of unsaturated soils: prediction and formulas. Methods of Soil Analysis: Part 1—Physical and Mineralogical Methods , 799–823.

Oh, S., Kim, Y.K., Kim, J.W., 2015. A modified van genuchten-mualem model of hydraulic conductivity in korean residual soils. Water 7, 5487–5502.

Or, D., Tuller, M., 1999. Liquid retention and interfacial area in variably saturated porous media: Upscaling from single-pore to sample-scale model. Water Resources Research 35, 3591–3605.

Petersen, E.E., 1958. Diffusion in a pore of varying cross section. AIChE Journal 4, 343–345.

Pham, H.Q., Fredlund, D.G., Barbour, S.L., 2005. A study of hysteresis models for soil-water characteristic curves. Canadian Geotechnical Journal 42, 1548–1568.

Reis, J.C., Acock, A.M., 1994. Permeability reduction models for the precipitation of inorganic solids in berea sandstone. In situ 18, 347–368.

Rembert, F., Jougnot, D., Guarracino, L., 2020. A fractal model for the electrical conductivity of water-saturated porous media during mineral precipitation-dissolution processes. Advances in Water Resources 145, 103742.

Soldi, M., Guarracino, L., Jougnot, D., 2017. A simple hysteretic constitutive model for unsaturated flow. Transport in Porous Media 120, 271–285.

Spiteri, E.J., Juanes, R., Blunt, M.J., Orr, F.M., et al., 2008. A new model of trapping and relative permeability hysteresis for all wettability characteristics. Spe Journal 13, 277–288.

Stanić, F., Cui, Y.J., Delage, P., De Laure, E., Versini, P.A., Schertzer, D., Tchiguirinskaia, I., 2020a. A device for the simultaneous determination of the water retention properties and the hydraulic conductivity function of an unsaturated coarse material; application to a green-roof volcanic substrate. Geotechnical Testing Journal 43.

Stanić, F., Delage, P., Tchiguirinskaia, I., Versini, P.A., Cui, Y.J., Schertzer, D., 2020b. A new fractal approach to account for capillary and adsorption phenomena in the water retention and transfer properties of unsaturated soils. Water Resources Research 56, e2020WR027808.

Thanh, L.D., Jougnot, D., Van Do, P., Van Nghia A, N., 2019. A physically based model for the electrical conductivity of water-saturated porous media. Geophysical Journal International 219, 866–876.

Topp, G.C., Miller, E.E., 1966. Hysteretic moisture characteristics and hydraulic conductivities for glass-bead media. Soil Science Society of America Journal 30, 156–162.

Tuller, M., Or, D., Dudley, L.M., 1999. Adsorption and capillary condensation in porous media: Liquid retention and interfacial configurations in angular pores. Water Resources Research 35, 1949–1964.

Tyler, S.W., Wheatcraft, S.W., 1990. Fractal processes in soil water retention. Water Resources Research 26, 1047–1054.

Van Genuchten, M.T., 1980. A closed-form equation for predicting the hydraulic conductivity of unsaturated soils. Soil Sci. Soc. Am. J 44, 892–898.

Vogel, H.J., Roth, K., 2001. Quantitative morphology and network representation of soil pore structure. Advances in water resources 24, 233–242.

Wang, S., Wu, T., Qi, H., Zheng, Q., Zheng, Q., 2015. A permeability model for power-law fluids in fractal porous media composed of arbitrary cross-section capillaries. Physica A: Statistical Mechanics and its Applications 437, 12–20, https://doi.org/10.1016/j.physa.2015.05.089.

Xu, C., Torres-Verdín, C., 2013. Pore system characterization and petrophysical rock classification using a bimodal gaussian density function. Mathematical Geosciences 45, 753–771.

Xu, P., Zhang, L., Rao, B., Qiu, S., Shen, Y., Wang, M., 2020. A fractal scaling law between tortuosity and porosity in porous media. Fractals 28, 2050025.

Yang, H., Rahardjo, H., Leong, E.C., Fredlund, D.G., 2004. Factors affecting drying and wetting soil-water characteristic curves of sandy soils. Canadian Geotechnical Journal 41, 908–920.

Yu, B., 2008. Analysis of flow in fractal porous media. Applied Mechanics Reviews 61, 050801.

Yu, B., Lee, L.J., Cao, H., 2002. A fractal in-plane permeability model for fabrics. Polymer composites 23, 201–221.

Yu, B., Li, J., 2001. Some fractal characters of porous media. Fractals 9, 365–372.

Yu, B., Li, J., Li, Z., Zou, M., 2003. Permeabilities of unsaturated fractal porous media. International journal of multiphase flow 29, 1625–1642.

Symbol	Description	Units
REV	Representative elementary volume	-
R	Radius of a circular tube	m
a	Radial factor of the constrictivity	-
c	Length factor of the constrictivity	-
λ	Wavelength	m
l	Pore length	m
$r(x)$	Pore radius variation along the longitudinal variable x	m
M	Integer number	-
V_p	Pore volume	m^3
f_v	Reduction factor in a pore volume and in the porosity	-
q_p	Pore volumetric water flow	$m^3\ s^{-1}$
Δh	Pressure head drop	m
f_k	Reduction factor in a pore volumetric water flow and in the permeability	-
R_{REV}	REV radius	m
L	REV length	m
τ	Tortuosity	-
$N(R)$	Number of pores of radius equal or larger than R	-
D	Fractal dimension	-
R_{min}	Minimum pore radius	m
R_{max}	Maximum pore radius	m
ϕ	Porosity	-
q	Volumetric water flow through the REV	$m^3\ s^{-1}$
k	Permeability	m^2
k_{rel}	Relative permeability	-
h	Pressure head	m
T_s	Surface tension	$N\ m^{-1}$
β	Contact angle	degrees
S_e	Effective saturation	-
S_e^d,S_e^w	Main drying and wetting effective saturation, respectively	-
h_{min}	Minimum pressure head	m
h_{max}	Maximum pressure head	m
k_{rel}^d,k_{rel}^w	Main drying and wetting relative permeability, respectively	-
ρ	Water density	$kg\ m^{-3}$
g	Gravity	$m\ s^{-2}$
μ	Water dynamic viscosity	Pa s